


# Development of Short-Range White Matter in Healthy Children and Adolescents

Adeoye A. Oyefiade,<sup>1,2</sup> Stephanie Ameis,<sup>1,3</sup> Jason P. Lerch,<sup>1</sup> Conrad Rockel,<sup>4</sup>  
Kamila U. Szulc,<sup>1</sup> Nadia Scantlebury,<sup>1</sup> Alexandra Decker,<sup>1</sup> Jaleel Jefferson,<sup>1</sup>  
Simon Spichak,<sup>5</sup> and Donald J. Mabbott <sup>1,2\*</sup>

<sup>1</sup>Neurosciences and Mental Health, The Hospital for Sick Children, Toronto, Ontario

<sup>2</sup>Department of Psychology, University of Toronto, Toronto, Ontario

<sup>3</sup>Campbell Family Mental Health Research Institute, The Center for Addictions and Mental Health, Toronto, Ontario

<sup>4</sup>Department of Medical Biophysics, Western University, London, Ontario

<sup>5</sup>Department of Human Biology, University of Toronto, Toronto, Ontario

---

**Abstract:** Neural communication is facilitated by intricate networks of white matter (WM) comprised of both long and short range connections. The maturation of long range WM connections has been extensively characterized, with projection, commissural, and association tracts showing unique trajectories with age. There, however, remains a limited understanding of age-related changes occurring within short range WM connections, or *U-fibers*. These connections are important for local connectivity within lobes and facilitate regional cortical function and greater network economy. Recent studies have explored the maturation of U-fibers primarily using cross-sectional study designs. Here, we analyzed diffusion tensor imaging (DTI) data for healthy children and adolescents in both a cross-sectional ( $n = 78$ ; mean age =  $13.04 \pm 3.27$  years) and a primarily longitudinal ( $n = 26$ ; mean age =  $10.78 \pm 2.69$  years) cohort. We found significant age-related differences in fractional anisotropy (FA), mean diffusivity (MD), axial diffusivity (AD) and radial diffusivity (RD) across the frontal, parietal, and temporal lobes of participants within the cross-sectional cohort. By contrast, we report significant age-related differences in only FA for participants within the longitudinal cohort. Specifically, larger FA values were observed with age in frontal, parietal, and temporal lobes of the left hemisphere. Our results extend previous findings restricted to long range WM to demonstrate regional changes in the microstructure of short range WM during childhood and adolescence. These changes possibly reflect continued myelination and axonal organization of short range WM with increasing age in more anterior regions of the left hemisphere. *Hum Brain Mapp* 00:000–000, 2017. © 2017 Wiley Periodicals, Inc.

**Key words:** short-range WM; DTI; white matter maturation; linear mixed effects model

---

Additional Supporting Information may be found in the online version of this article.

Contract grant sponsor: Canadian Cancer Society Research Institute; Contract grant number: 2012-701423; Contract grant sponsor: Canadian Institute for Health Research (CIHR); Contract grant number: 123537

\*Correspondence to: Donald J. Mabbott, Neurosciences and Mental Health, The Hospital for Sick Children, Toronto, Ontario.  
E-mail: Donald.mabbott@sickkids.ca

Received for publication 8 March 2017; Revised 14 September 2017; Accepted 25 September 2017.

DOI: 10.1002/hbm.23836

Published online 00 Month 2017 in Wiley Online Library (wileyonlinelibrary.com).

## INTRODUCTION

Cognitive development is linked with the maturation of white matter [Nagy et al., 2004]. As such a detailed understanding of white matter maturation across the *entire* brain is critical to advancing our understanding of both typical and atypical cognitive development. White matter can be broadly divided into short and long range connections. Long-range connections are comprised of commissural, projection, and association fibers that connect distant brain regions and facilitate the transfer of multimodal sensory information from subcortical nuclei to sensory and association cortices [Mesulam, 1990]. Short-range connections, on the other hand, are comprised of fibers that connect neighboring grey matter regions within lobes. These connections were first described as white matter fibers that rest just beneath the cortex and connect adjacent cortical areas by following the convexity of gyral convolutions in the form of “U”-shaped fibers or long intralobar fibers [Meynert, 1885]. Recent structural investigations in nonhuman primates using axon staining techniques [Yeterian et al., 2012] and in adult human brains using white matter imaging methods and post-mortem dissections [Catani et al., 2012] have shown that short-range connections are primarily intra-lobar, connecting brain regions in close physical proximity with each other. Highly interconnected regions within lobes, or modules, are an integral part of brain network architecture as they may conserve resources otherwise required to process information over longer distances [Bullmore and Sporns, 2012]. Therefore, short-range connections are particularly important during development as they may allow for a closely negotiated compromise between the increased network cost provided by modules and the greater network efficiency provided by long-range connections [Sporns, 2013]. Neuroimaging studies to date have largely focused on age-related changes in long-range white matter connections. Currently, little is known about the maturation of short-range white matter connections in childhood and adolescence.

DTI is a magnetic resonance imaging-based technique that enables the examination of white matter microstructure via the diffusion of water molecules across fatty tissue in the brain [Basser, 1995]. Scalar values ( $\lambda_1$ ,  $\lambda_2$ , and  $\lambda_3$ ) derived from the diffusion tensor describe the extent to which water diffusion is restricted within a given image voxel [Le Bihan et al., 2001]. Secondary parameters can be extracted from these values—fractional anisotropy [FA], radial diffusivity [RD], axial diffusivity [AD], and mean diffusivity [MD]—that provide indirect information about the microstructure of underlying white matter connections [Basser et al., 2000; Song et al., 2002; Song et al., 2003]. Human and animal studies have demonstrated that in regions where there are minimal partial volume effects and/or few crossing fibers, larger FA values with age reflect increase in white matter microstructure and organization [Assaf and Pasternak, 2008]. Smaller RD and AD values may reflect in part myelination and axonal

thickness [Song et al., 2003]. Smaller MD values may reflect reduced water content and WM density [Barnea-Goraly et al., 2005; Mukherjee et al., 2001]. Prior studies have demonstrated larger FA and smaller MD and RD in long range connections with age [Lebel and Beaulieu, 2011; Lebel et al., 2008; Sowell et al., 1999; Thompson et al., 2000]. Projection and commissural fibers show plateaued DTI measures by adolescence, while association fibers continue to mature well into adulthood [Lebel and Beaulieu, 2011].

Studies of aging in cross-sectional samples of adults have suggested that short range WM may have unique patterns of age-related difference depending on location in the brain [Nazeri et al., 2015; Phillips et al., 2013]. Generally, lower FA and higher MD, RD, and AD is observed with increasing age across the entire brain, with differences most pronounced in anterior as opposed to posterior areas. These findings suggest that short range connections in frontal areas may be more vulnerable to the aging process than those in other parts of the brain [Nazeri et al., 2015; Phillips et al., 2013]. Few studies have examined maturation of short range WM in children and adolescents. Wu et al. (2014) investigated age-related differences in DTI measures of short range WM in a cross-sectional sample of 133 healthy children and adolescents aged 10–18 years. They found distinct patterns of age-related differences in micro-regions within lobes; higher FA and lower MD and RD was observed with greater age in some areas while higher FA coincided with higher AD with age in other areas.

In the present study, we examined age-related differences in short range WM using both cross-sectional and longitudinal data. In particular, we sought to identify age-related differences in short range WM in a cross-sectional cohort of children/adolescents scanned in a 3 Tesla scanner, and to validate these changes in a separate primarily longitudinal cohort of children/adolescents scanned in a 1.5 Tesla scanner. We hypothesize that the most robust age-related differences will be evident across cohorts scanned at different field strengths, particularly greater FA and lower MD and RD with age for short range WM across the brain. We also qualitatively explored whether the greatest age-related differences were evident in anterior versus posterior regions.

## MATERIALS AND METHODS

### Participant Characteristics

Participant data was retrieved from pre-existing databases of healthy children and adolescents recruited as part of larger studies at the Hospital for Sick Children. Participants were excluded if they had a premorbid history of developmental delay, learning disability, psychiatric/neurological disorder, or traumatic brain injury. Magnetic resonance (MR) measurements from 104 participants were

**TABLE I. Participant characteristics**

	Cross-sectional cohort	Longitudinal cohort	Cohort differences ( <i>P</i> )
Number of subjects (females)	78 (28)	26 (13) <sup>a</sup>	-
Number of scans (females)	78 (28)	51 (23)	-
Handedness (left)	72 (6)	20 (6)	-
Mean age (cohort)	13.04 ± 3.27 years	10.78 ± 2.69 years	<0.0001
Mean age Females	13.05 ± 3.19 years	10.46 ± 2.55 years	0.003
Mean age Males	13.03 ± 3.34 years	11.06 ± 2.81 years	0.01
Intracranial Volume (ICV)	1.51 ± 0.13 litres	1.51 ± 0.11 litres	0.71
MRI scan type	3 Tesla	1.5 Tesla	-

<sup>a</sup>Eight subjects were scanned once in this cohort.

retrieved for this study. Participant data was grouped into two cohorts. Participants in the first cohort (solely cross-sectional) were aged from 5.15 to 18.97 years with a mean age of 13.04 ± 3.27 years. There were 78 participants in total within this cohort (50 males and 28 females) and the majority of participants were right-handed (*n* = 74). These participants were scanned once using a 3 Tesla Siemens scanner (Table I, Fig. 1). Participants in the second cohort (primarily longitudinal) were aged from 5.75 to 16.92 years at the time of first scan, with a mean age of 10.23 ± 2.74 years. There were 26 participants in total within this cohort (13 males and 13 females) and the majority of participants were right-handed (*n* = 23). These participants were scanned on a 1.5 Tesla GE MRI scanner, with a majority of participants (75%) receiving 2–3 chronologically concurrent scans at least a year apart (Fig. 1). The participants in the first cohort were older than those in the second cohort (*P* < 0.0001). There was no difference in age between males and females in either the first (*P* = 0.98) or the second cohort (*P* = 0.44). Access to participant databases was approved by the research ethics board at the Hospital for Sick Children.

### MR Image Acquisition and Processing

**First Cohort:** MR measurements from this cohort were acquired at the Hospital for Sick Children using a Siemens 3 Tesla whole-body MRI scanner (TrioTim syngo MR B17 system) with a twelve-channel head coil. The scanning protocol included a 3D—T1 magnetization prepared 180 degrees' radio-frequency pulse and a rapid gradient-echo (MPRAGE) sequence with the following parameters: TE/TR = 3.91/2,300 ms, 160 contiguous axial slices, flip angle = 90°, 256 × 244 matrix, FOV = 256 × 224 mm, voxel size = 1 mm ISO. Diffusion tensor data was acquired using a single shot spin echo sequence with the following parameters: 30 directions, *b* = 1,000 s/mm<sup>2</sup>, TE/TR = 90/9,000 ms, 70 contiguous axial slices, flip angle = 90°, 122 × 122 matrix interpolated to 244 × 244, FOV = 244 × 244 mm, voxel size = 2 mm ISO.

**Second Cohort:** MR measurements from this cohort were acquired at the Hospital for Sick Children using a

GE LX 1.5 Tesla MRI scanner with an eight-channel head coil (GE Healthcare, Milwaukee, Wis). The scanning protocol included a 3D—T1 fast-spoiled gradient-echo (FSPGR) inversion recovery-prepared sequence with the following parameters: TE/TR = 4.2/10,056 ms, 116–124 contiguous axial slices, flip angle = 90°, NEX = 1, 256 × 192 matrix interpolated to 256 × 256, FOV = 240 × 240 mm, receive bandwidth = 162.734 kHz, slice thickness = 1.5 mm. Diffusion tensor data was acquired using a single-shot spin-echo DTI sequence with the following parameters: 30 directions, *b* = 1,000 s/mm<sup>2</sup>, TE/TR = 84.6/15,000 ms, 45–50 contiguous axial slices, flip angle = 90°, NEX = 1, 128

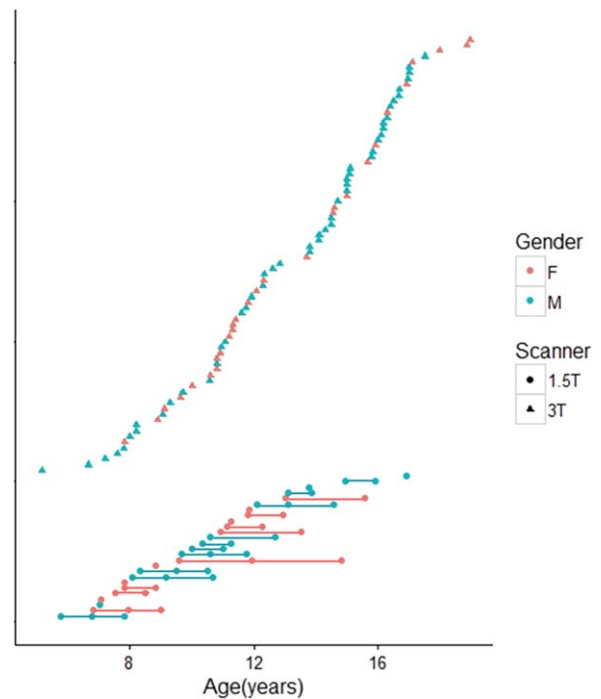


**Figure 1.**

Age distribution of healthy subjects at the time of image acquisition. Participants for whom concurrent MR scans were acquired are shown at the bottom of the chart. [Color figure can be viewed at [wileyonlinelibrary.com](http://wileyonlinelibrary.com)]

× 128 matrix interpolated to 256 × 256, FOV = 240 × 240 mm, receive bandwidth = 1,953.12 kHz, slice thickness = 3 mm.

All images were corrected for inhomogeneity and eddy currents, and processed using the functional magnetic resonance imaging of the brain (fMRIB) Software Library (FSL) [Behrens et al., 2003, 2007; Smith et al., 2004; Woolrich et al., 2009] and ANALYZE™ Imaging Software (Biomedical Imaging Resource, Mayo Foundation) We manually masked out nonbrain tissue from T1 and diffusion-weighted scans in ANALYZE™ (Fig. 2). Brain-extracted T1 images were automatically classified into grey matter, white matter, and cerebrospinal fluid using the automatic tissue segmentation algorithm FSL-FAST (fMRIB Automated Segmentation Tool) [Zhang et al., 2001]. The image intensities of brain-extracted T1 images were inverted to highlight the CSF, which allowed for better co-registration with diffusion-weighted images. Co-registration of T1 and diffusion-weighted images was achieved by way of a twelve-dimension linear transformation, followed by nonlinear warping using a second-order nonlinear parameter model [Woods et al., 1998]. Co-registration produced a T1-to-DTI transformation matrix that enabled the transformation of T1 anatomical information into DTI space. White matter segmentations on T1 images were subdivided into compartments using a well-validated anatomic template [Mazziotta et al., 2001]. The template consisted of eight cerebral (bilateral frontal, parietal, temporal, and occipital hemispheric) and four posterior fossa (pontine, vermal, and bilateral cerebellar hemispheric) regions. Specifically, the template was applied to the T1 of all subjects by way of affine transformation [Woods et al., 1998]. Compartmentalized T1 scans were registered to the previously created T1-to-DTI matrices using linear and nonlinear transformations to delineate white matter compartments within DTI space [Mabbott et al., 2009]. For each scan, this template-derived compartmentalized image served as the source image in the estimation of short range white matter across the cerebrum.

### Estimation of Short-Range White Matter

The same protocol for estimating short-range WM measures was used for both cohorts. As short-range white matter is primarily intra-lobar, we approached short-range tract estimation in 2 stages; (a) we estimated all possible white matter tracts within each lobe using probabilistic tractography, (b) we delineated short-range tracts from all possible connections by applying a thresholding protocol to all delineated tracts. Tracts were seeded from a region of interest (ROI) which corresponded to each cerebral lobe within a given hemisphere. Seed ROI's were created by applying each individual's template-derived T1-to-DTI matrix to zero diffusion images by way of affine transformation (Fig. 3). This resulted in the parcellation of individual brains into discrete lobar regions. Prior to

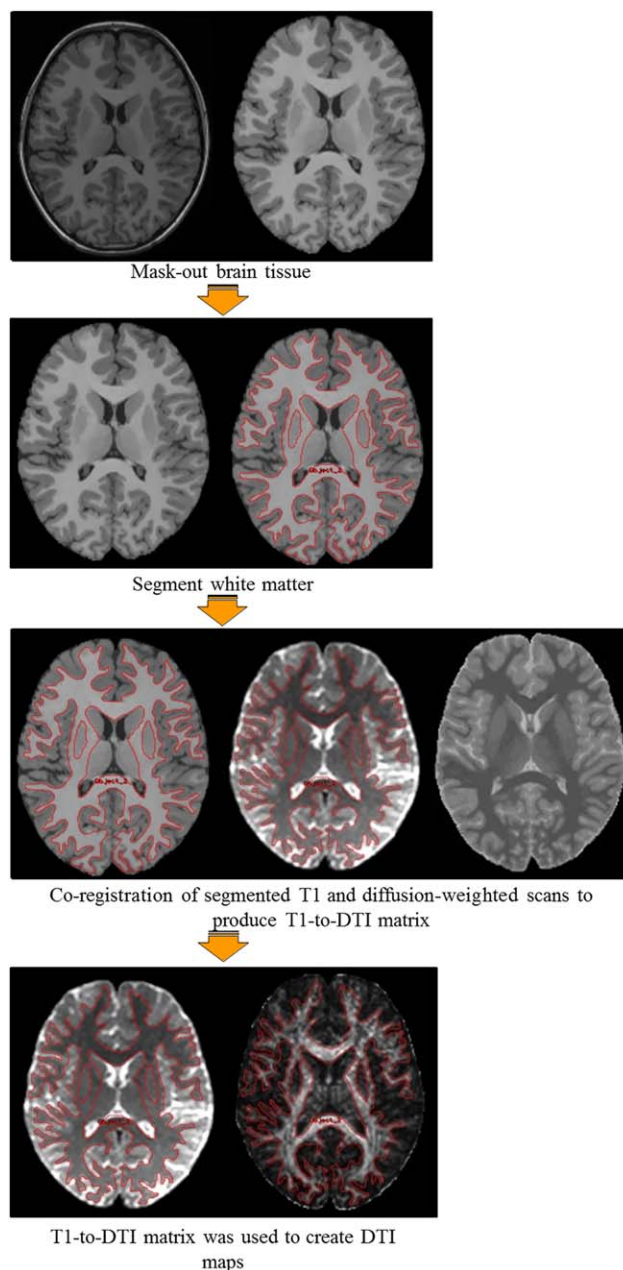


**Figure 2.**

A brief summary of the processing stream used to derive DTI measures. Extraction of brain tissue and segmentation of white matter on T1 and diffusion-weighted scans was followed by an affine co-registration process to produce T1-to-DTI transformation matrices. These matrices were used to compartmentalize cerebral white matter and to create DTI maps from which DTI indices were calculated.

tractography, lobar ROI's were isolated and applied to zero diffusion images in order to create exclusion masks wherein all other white matter tracts were to be excluded (see Supporting Information Fig. S1 for a full

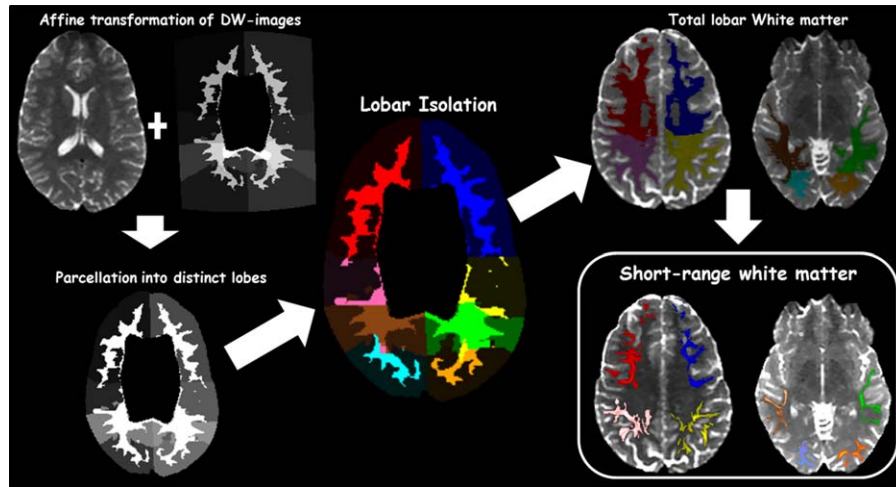


**Figure 3.**

A summary of the analysis pipeline used for short range WM delineation. Diffusion-weighted (DW) images were parcellated into discrete lobar regions using a template-derived T1-to-DTI transformation matrix. All possible WM tracts within each lobe were delineated using probabilistic tractography. Elimination of

illustration). Probabilistic tractography was performed using the FSL Probtrackx tool [Behrens et al., 2003, 2007] to delineate white matter tracts within each lobe (Fig. 3). Short range WM connect adjacent gyri within lobes and tend to have a characteristic “U” shape that may be either short (connecting neighboring intra-lobar gyri) or elongated (connecting more distant intra-lobar gyri). To enable visual identification of short-range white matter, we applied a thresholding protocol aimed at pruning the total number of probabilistic streamlines passing through all the voxels in a given lobe. First, we ignored spurious streamlines to minimize the effect of outliers on tract estimation [Jenkinson et al., 2012; Smith et al., 2004]. Next, we assessed the effect of eliminating streamlines in a step-wise fashion on the visualization of short-range tracts. We segmented a subset of our data ( $n = 26$ ) at predefined fractions of total number of probabilistic streamlines passing through all nonzero voxels (10–90%). Following visual inspection and qualitative inter-rater consensus by multiple raters (S.A, C.R, and A.O), short-range tracts were best observed when 60% of the total number of probabilistic streamlines was removed (Fig. 3). Subsequently, we thresholded all delineated tracts within each lobe, and calculated DTI measures (FA, MD, AD, and RD) by averaging across all nonzero voxels.

### Statistical Analyses

We modeled the developmental trajectory of short range white matter by analyzing age-related changes in DTI indices across the brain. As prior research has shown that normal white matter development may follow linear and curvilinear patterns of age-related change [Lebel and

60% of probabilistic streamlines revealed short range WM tracts within each lobe. Color codes: Right hemisphere—frontal (red), parietal (pink), temporal (brown), occipital (cyan). Left hemisphere—frontal (blue), parietal (yellow), temporal (green), occipital (orange).

Beaulieu, 2011; Lebel et al., 2008], we considered  $age$ ,  $age^2$ , and  $age^3$  terms in our models. We computed whole-lobe indices for the entire frontal, parietal, temporal, and occipital lobes by averaging corresponding left and right hemisphere lobes. Model fits were calculated for the entire frontal, parietal, temporal, and occipital lobes. Separate fits were also calculated for left and right hemisphere frontal, parietal, temporal, and occipital lobes. Participant sex, handedness, and intracranial volume (ICV) were included as covariates in each model. Intracranial volume was obtained by calculating the total volume (in  $mm^3$ ) of all nonzero voxels in brain-extracted T1 images. To better account for overall white matter change with age, we initially analyzed age-related changes in each lobe as a function of overall FA, MD, AD, and RD. Residuals obtained from these models represent the proportion of short range WM information not explained by whole-brain white matter. We included these residuals as covariates in our analyses to control for information obtained from overall WM change with age (wb).

For data from the first cohort (cross-sectional data), we analyzed age-related changes in each DTI index using a general linear model:

$$DTI\ index = A \cdot age + A \cdot age^2 + A \cdot age^3 + B \cdot sex + C \cdot hand + D \cdot ICV + E \cdot wb + \epsilon.$$

For data from the second cohort (primarily longitudinal data), we analyzed age-related changes in each DTI index using a linear mixed-effects model:

$$DTI\ index = (A + S_A) \cdot age + (A + S_A) \cdot age^2 + (A + S_A) \cdot age^3 + B \cdot sex + C \cdot hand + D \cdot ICV + E \cdot wb + \epsilon.$$

For the second model, the error term ‘ $\epsilon$ ’ includes deviations from model predictions due to the random variation associated with participant age.  $S_A$  in the age term accounted for this variability, representing the participant-specific random intercept and slope terms for the age variable. A random intercept term increased the expressivity of our models by allowing predictions to vary across participants, while a random slope term captured variation in the rate of change in DTI indices across participants. The inclusion of random intercept and slope terms ensured that sources of random variation associated with the age variable were captured within model estimates. Additionally, it was necessary for practical reasons to simplify the random effect structure of our model as estimation procedures for complex linear mixed-effect models often fail to converge in a reasonable amount of iterations [Barr et al., 2013; Bolker et al., 2009]. To enable model convergence, we ignored correlations between random intercept and slope terms. All model estimations and  $p$  value calculations were done in R using the lme4 package [Bates et al., 2015]. The lme4 package uses a Satterthwaite approximation to degrees of freedom and calculates  $p$  values from sequential tests of all effects in the model. We applied a False Discovery Rate (FDR) adjustment to  $p$  values in order to correct for multiple comparisons. Whereas  $p$  values estimate the proportion of truly null features that are called significant, FDR-adjusted  $p$  values, or  $q$  values, estimate the proportion of significant features that are truly null [Benjamini and Hochberg, 1995; Yekutieli and Benjamini, 1999]. For the purposes of our study, features with  $q$  values  $\leq 5\%$  were called significant. Initial analyses revealed significant effects of age for only linear models (Supporting Information Tables S1 and S2). We therefore dropped nonlinear terms from model fits in the final analyses.

## RESULTS

### Whole-Lobe and Hemispheric Changes in Short Range WM within the Cross-Sectional Cohort

Age-related differences in DTI measures were observed in every lobe except the occipital lobes (Table IIa). FA was larger in older versus younger children/adolescents in frontal, parietal, and temporal lobes (Frontal: slope = 0.0031,  $q = 0.023$ ,  $R^2 = 0.06$ . Parietal: slope = 0.0025,  $q = 0.049$ ,  $R^2 = 0.05$ . Temporal: slope = 0.0027,  $q = 0.0434$ ,  $R^2 = 0.08$ ) (Fig. 4). MD was smaller in older versus younger participants in the frontal (slope =  $-6.27 \times 10^{-6} \text{ mm}^2 \text{ s}^{-1} \text{ yr}^{-1}$ ,  $q < 0.0001$ ,  $R^2 = 0.4$ ), parietal (slope =  $-3.75 \times 10^{-6} \text{ mm}^2 \text{ s}^{-1} \text{ yr}^{-1}$ ,  $q < 0.0001$ ,  $R^2 = 0.21$ ) and temporal lobes (slope =  $-3.32 \times 10^{-6} \text{ mm}^2 \text{ s}^{-1} \text{ yr}^{-1}$ ,  $q = 0.003$ ,  $R^2 = 0.11$ ) (Fig. 5). Likewise, RD was smaller in the frontal (slope =  $-6.30 \times 10^{-6} \text{ mm}^2 \text{ s}^{-1} \text{ yr}^{-1}$ ,  $q < 0.001$ ,  $R^2 = 0.28$ ), parietal (slope =  $-4.00 \times 10^{-6} \text{ mm}^2 \text{ s}^{-1} \text{ yr}^{-1}$ ,  $q = 0.0011$ ,  $R^2 = 0.14$ ) and temporal lobes (slope =  $-3.98 \times 10^{-6} \text{ mm}^2$

$\text{s}^{-1} \text{ yr}^{-1}$ ,  $q = 0.0012$ ,  $R^2 = 0.16$ ) (Fig. 7). Lower AD in older versus younger participants was observed in only the frontal and parietal lobes (Frontal: slope =  $-6.20 \times 10^{-6} \text{ mm}^2 \text{ s}^{-1} \text{ yr}^{-1}$ ,  $q < 0.001$ ,  $R^2 = 0.24$ . Parietal: slope =  $-3.19 \times 10^{-6} \text{ mm}^2 \text{ s}^{-1} \text{ yr}^{-1}$ ,  $q = 0.049$ ,  $R^2 = 0.12$ ) (Fig. 6).

Regional analyses within each hemisphere revealed larger FA in older versus younger participants in the frontal and temporal lobes of the left hemisphere (Frontal: left slope = 0.004,  $q = 0.003$ ; right slope = 0.002;  $q = 0.14$ . Temporal: left slope = 0.003,  $q = 0.02$ ; right slope = 0.002;  $q = 0.15$ ) (Table IIb). We also found larger age-related differences for FA in the parietal lobes of the right hemisphere but not the left (left slope = 0.002,  $q = 0.22$ ; right slope = 0.003;  $q = 0.02$ ). MD was lower in older versus younger participants in bilateral frontal (left slope =  $-7.47 \times 10^{-6} \text{ mm}^2 \text{ s}^{-1} \text{ yr}^{-1}$ ,  $q < 0.0001$ ; right slope =  $-5.06 \times 10^{-6} \text{ mm}^2 \text{ s}^{-1} \text{ yr}^{-1}$ ,  $q < 0.0001$ ), parietal (left slope =  $-2.67 \times 10^{-6} \text{ mm}^2 \text{ s}^{-1} \text{ yr}^{-1}$ ,  $q = 0.02$ ; right slope =  $-4.81 \times 10^{-6} \text{ mm}^2 \text{ s}^{-1} \text{ yr}^{-1}$ ;  $q < 0.0001$ ), and temporal lobes (left slope =  $-2.22 \times 10^{-6} \text{ mm}^2 \text{ s}^{-1} \text{ yr}^{-1}$ ,  $q = 0.07$ ; right slope =  $-4.41 \times 10^{-6} \text{ mm}^2 \text{ s}^{-1} \text{ yr}^{-1}$ ;  $q = 0.0003$ ). RD was also lower in bilateral frontal (left slope =  $-7.71 \times 10^{-6} \text{ mm}^2 \text{ s}^{-1} \text{ yr}^{-1}$ ,  $q < 0.0001$ ; right slope =  $-4.67 \times 10^{-6}$ ;  $q = 0.0002$ ), parietal (left slope =  $-2.71 \times 10^{-6} \text{ mm}^2 \text{ s}^{-1} \text{ yr}^{-1}$ ,  $q = 0.05$ ; right slope =  $-4.67 \times 10^{-6} \text{ mm}^2 \text{ s}^{-1} \text{ yr}^{-1}$ ;  $q = 0.003$ ), and temporal lobes (left slope =  $-3.64 \times 10^{-6} \text{ mm}^2 \text{ s}^{-1} \text{ yr}^{-1}$ ,  $q = 0.005$ ; right slope =  $-4.3 \times 10^{-6} \text{ mm}^2 \text{ s}^{-1} \text{ yr}^{-1}$ ;  $q = 0.001$ ). AD was lower in the frontal lobes of the left hemisphere (Frontal: left slope =  $-7.02 \times 10^{-6} \text{ mm}^2 \text{ s}^{-1} \text{ yr}^{-1}$ ,  $q = 0.0003$ ) as well as in the frontal, parietal, and temporal lobes of the right hemisphere (Frontal: right slope =  $-5.67 \times 10^{-6} \text{ mm}^2 \text{ s}^{-1} \text{ yr}^{-1}$ ,  $q = 0.0006$ . Parietal: right slope =  $-3.79 \times 10^{-6} \text{ mm}^2 \text{ s}^{-1} \text{ yr}^{-1}$ ,  $q = 0.05$ . Temporal: right slope =  $-4.60 \times 10^{-7} \text{ mm}^2 \text{ s}^{-1} \text{ yr}^{-1}$ ,  $q = 0.03$ ).

### Whole-Lobe and Hemispheric Changes in Short-Range WM within the Primarily Longitudinal Cohort

For the second cohort, we found significant age-related increases in FA in the frontal lobes (Frontal: slope = 0.0031,  $q = 0.034$ ,  $R^2 = 0.25$  (Table IIIa). Regional analyses within each hemisphere showed significant age-related increases in FA in the frontal, parietal, and temporal lobes of the left hemisphere (Frontal: left slope = 0.0035,  $q = 0.03$ . Parietal: left slope = 0.0046,  $q = 0.03$ . Temporal: left slope = 0.0048,  $q = 0.03$ ) (Table IIIb). There were no significant changes in MD, AD, and RD within this cohort.

### Qualitative Comparison of Trajectories between Cohorts

Whole-lobe maturational trajectories between both cohorts are presented in Figures 4–7. We observed similar trends of increasing FA and decreasing MD, AD, and RD in the frontal, parietal, and temporal lobes of both cohorts. However, different trends were observed for the occipital

◆ Short-Range White Matter in Children and Adolescents ◆

**TABLE II. Age-related differences in (a) whole-lobe and (b) hemispheric DTI measures across the brain for participants in the cross-sectional cohort**

a								
DTI measure	Intercept	Slope	SE	$R^2$	$P$	$q$		
FA								
Frontal	0.325	0.0031	0.0012	0.06	0.018	<b>0.023</b>		
Parietal	0.310	0.0025	0.0011	0.05	0.074	<b>0.049</b>		
Temporal	0.274	0.0027	0.0012	0.08	0.012	<b>0.043</b>		
Occipital	0.226	0.0010	0.0013	0.02	0.607	0.539		
MD								
	mm <sup>2</sup> /s	mm <sup>2</sup> /s/year						
Frontal	0.0008	$-6.27 \times 10^{-6}$	$8.74 \times 10^{-7}$	0.40	$5.67 \times 10^{-10}$	<b>&lt;0.0001</b>		
Parietal	0.0008	$-3.75 \times 10^{-6}$	$8.78 \times 10^{-7}$	0.21	$6.07 \times 10^{-5}$	<b>&lt;0.001</b>		
Temporal	0.0009	$-3.32 \times 10^{-6}$	$9.91 \times 10^{-7}$	0.11	0.0013	<b>0.003</b>		
Occipital	0.0008	$-6.13 \times 10^{-7}$	$1.14 \times 10^{-6}$	-	0.593	0.633		
AD								
	mm <sup>2</sup> /s	mm <sup>2</sup> /s/year						
Frontal	0.0011	$-6.20 \times 10^{-6}$	$1.37 \times 10^{-6}$	0.24	$2.30 \times 10^{-5}$	<b>&lt;0.001</b>		
Parietal	0.0011	$-3.19 \times 10^{-6}$	$1.48 \times 10^{-6}$	0.12	0.034	<b>0.049</b>		
Temporal	0.0011	$-1.99 \times 10^{-6}$	$1.79 \times 10^{-6}$	0.01	0.090	0.120		
Occipital	0.0010	$-8.34 \times 10^{-6}$	$1.32 \times 10^{-6}$	0.04	0.530	0.606		
RD								
	mm <sup>2</sup> /s	mm <sup>2</sup> /s/year						
Frontal	0.0007	$-6.30 \times 10^{-6}$	$1.10 \times 10^{-6}$	0.28	$2.12 \times 10^{-7}$	<b>&lt;0.0001</b>		
Parietal	0.0007	$-4.00 \times 10^{-6}$	$1.07 \times 10^{-6}$	0.14	0.0004	<b>0.0011</b>		
Temporal	0.0007	$-3.98 \times 10^{-6}$	$1.08 \times 10^{-6}$	0.15	0.0005	<b>0.0012</b>		
Occipital	0.0007	$-4.98 \times 10^{-7}$	$1.44 \times 10^{-6}$	-	0.731	0.731		
b								
DTI measure	Left hemisphere				Right hemisphere			
	Intercept	Slope	$R^2$	$q$	Intercept	Slope	$R^2$	$q$
FA								
Frontal	0.355	0.004	0.11	<b>0.003</b>	0.391	0.002	0.02	0.14
Parietal	0.357	0.002	0.01	0.22	0.323	0.003	0.12	<b>0.02</b>
Temporal	0.332	0.003	0.10	<b>0.02</b>	0.357	0.002	0.03	0.15
Occipital	0.337	0.001	-	0.57	0.300	0.001	-	0.55
MD								
	mm <sup>2</sup> /s	mm <sup>2</sup> /s/yr ( $\times 10^{-6}$ )			mm <sup>2</sup> /s	mm <sup>2</sup> /s/yr ( $\times 10^{-6}$ )		
Frontal	0.00088	-7.47	0.37	<b>&lt;0.0001</b>	0.00082	-5.06	0.29	<b>&lt;0.0001</b>
Parietal	0.00083	-2.67	0.10	<b>0.02</b>	0.00088	-4.81	0.22	<b>0.0001</b>
Temporal	0.0009	-2.22	0.02	<b>0.07</b>	0.00089	-4.41	0.19	<b>0.0003</b>
Occipital	0.00079	-1.28	-	0.37	0.00084	0.06	-	0.98
AD								
	mm <sup>2</sup> /s	mm <sup>2</sup> /s/yr ( $\times 10^{-6}$ )			mm <sup>2</sup> /s	mm <sup>2</sup> /s/yr ( $\times 10^{-6}$ )		
Frontal	0.0012	-7.02	0.17	<b>0.0003</b>	0.0012	-5.35	0.21	<b>0.0006</b>
Parietal	0.0012	-2.57	0.12	0.14	0.0012	-3.79	0.07	<b>0.05</b>
Temporal	0.0012	-0.60	-	0.82	0.0012	-4.60	0.05	<b>0.03</b>
Occipital	0.0011	-1.70	0.01	0.31	0.0011	-7.06	-	0.98
RD								
	mm <sup>2</sup> /s	mm <sup>2</sup> /s/yr ( $\times 10^{-6}$ )			mm <sup>2</sup> /s	mm <sup>2</sup> /s/yr ( $\times 10^{-6}$ )		
Frontal	0.00070	-7.71	0.02	<b>&lt;0.0001</b>	0.00064	-4.67	0.17	<b>0.0003</b>
Parietal	0.00066	-2.71	0.02	<b>0.05</b>	0.00072	-5.28	0.23	<b>0.0001</b>
Temporal	0.00074	-3.64	0.11	<b>0.005</b>	0.00071	-4.3	0.17	<b>0.001</b>
Occipital	0.00064	-1.10	-	0.57	0.00070	0.48	-	0.98

SE—Standard error of slope.

$q$ —FDR-adjusted  $p$ -values. Values that survived FDR correction are bolded.

lobes in both cohorts. For the first cohort we observed smaller slopes for DTI measures in the occipital lobes (FA: 0.001, MD:  $-6.13 \times 10^{-7}$  mm<sup>2</sup>s<sup>-1</sup>yr<sup>-1</sup>, AD:  $-8.34 \times 10^{-7}$  mm<sup>2</sup>s<sup>-1</sup>yr<sup>-1</sup>, RD:  $-4.98 \times 10^{-7}$  mm<sup>2</sup>s<sup>-1</sup>yr<sup>-1</sup>). For the second cohort, we observed larger slopes for DTI measures in the occipital lobes (FA: 0.0034, MD:  $-4.01 \times 10^{-6}$  mm<sup>2</sup>s<sup>-1</sup>yr<sup>-1</sup>, AD:  $-1.99 \times 10^{-6}$  mm<sup>2</sup>s<sup>-1</sup>yr<sup>-1</sup>, RD:  $-4.38 \times 10^{-6}$  mm<sup>2</sup>s<sup>-1</sup>yr<sup>-1</sup>). Although not significant, larger values in the second cohort show that data from the primarily longitudinal cohort is more sensitive to age-related changes in short range WM within the occipital lobes.

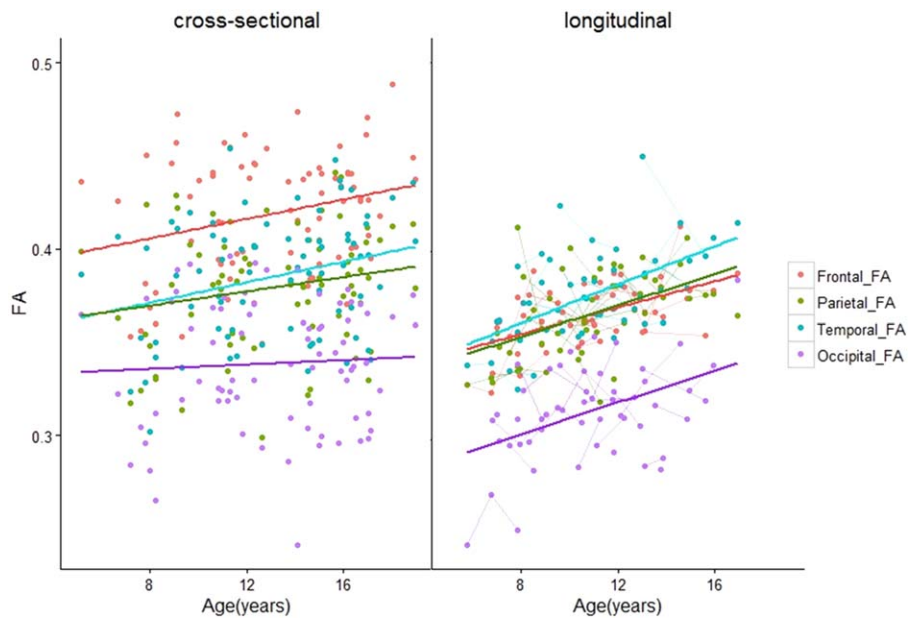


**Figure 4.**

Age-related changes in FA of short range WM across the brain. The different trajectories within each lobe are color-coded, while repeated scans per individual are shown in the longitudinal plot. In contrast to the rest of the brain, we did not observe significant age-related changes in FA in the occipital lobes of participants in the cross-sectional cohort. [Color figure can be viewed at [wileyonlinelibrary.com](http://wileyonlinelibrary.com)]

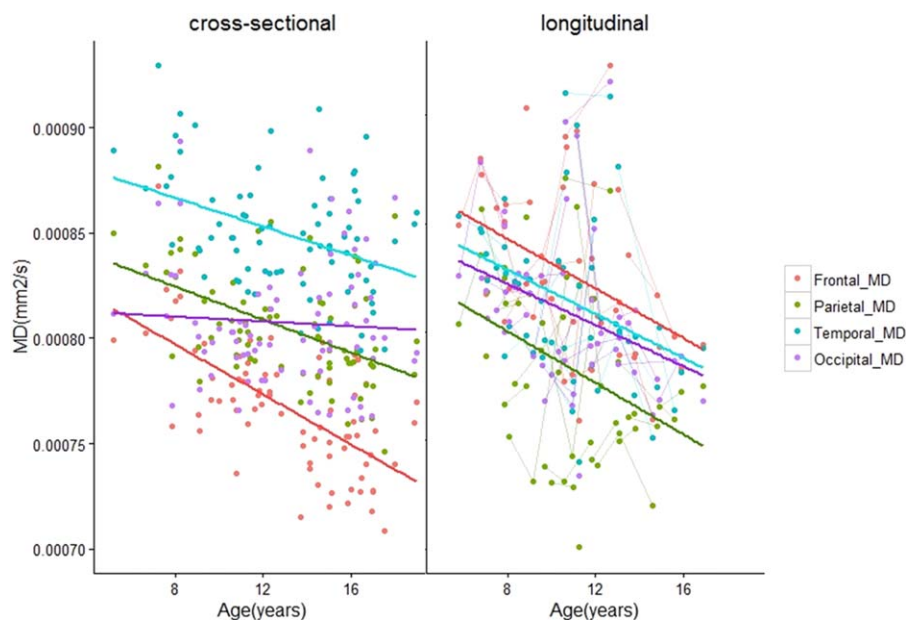


**Figure 5.**

Age-related changes in MD of short range WM across the brain. There were no age-related changes in MD in the occipital lobes of participants in the cross-sectional cohort. [Color figure can be viewed at [wileyonlinelibrary.com](http://wileyonlinelibrary.com)]



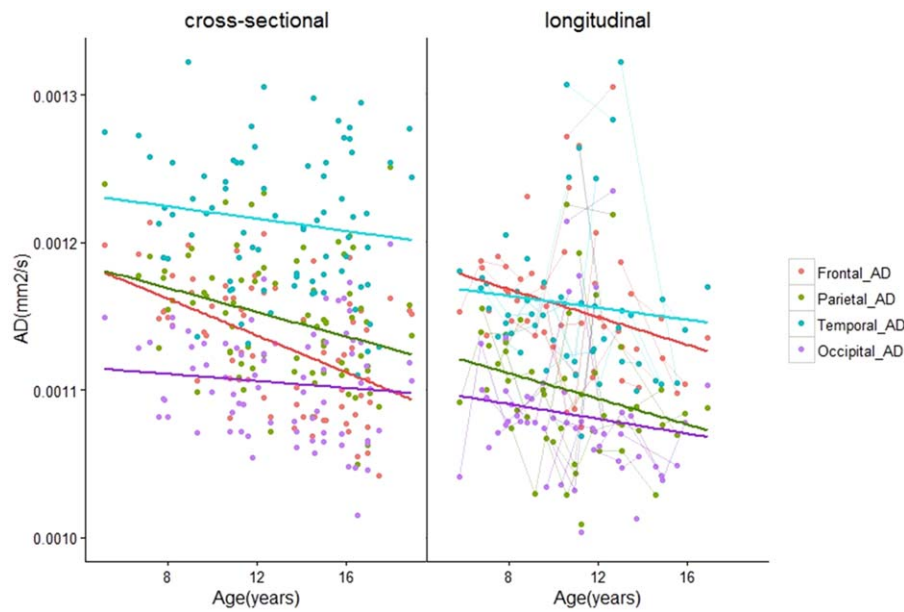


Figure 6. Age-related changes in AD of short range WM across the brain.

**Figure 6.**

Age-related changes in AD of short range WM across the brain. [Color figure can be viewed at [wileyonlinelibrary.com](http://wileyonlinelibrary.com)]

## DISCUSSION

Most studies exploring white matter maturation in childhood/adolescence have utilized cross-sectional approaches. These studies have found larger FA and smaller MD, AD, and RD with increasing age across developing long range WM tracts [Barnea-Goraly et al., 2005; Eluvathingal et al., 2007; Mukherjee et al., 2001]. More recent studies have utilized a longitudinal approach to explore WM development in children/adolescents and young adults, and have found both linear and nonlinear age-related increases in FA and decreases in MD, AD, and RD across long range WM [Lebel and Beaulieu, 2011; Lebel et al., 2008]. We extended these findings to short-range WM across the cerebrum in a sample of healthy children and adolescents by analyzing age-related differences in DTI measures acquired from cross-sectional and primarily longitudinal cohorts. For participants in the cross-sectional cohort we found significantly larger FA in the frontal, parietal, and temporal lobes, and smaller MD, and RD in the frontal, parietal, and temporal lobes. Changes in FA in the frontal and temporal lobes were lateralized to the left hemisphere, while changes in FA in the parietal lobes were lateralized to the right hemisphere. Changes in MD, AD, and RD were observed bilaterally. We validated findings from the cross-sectional cohort by examining similar changes in DTI measures within a primarily longitudinal cohort of participants. We found significant age-related increases in FA in the frontal, parietal, and temporal lobes which were lateralized to the left

hemisphere. Importantly, these effects are observed after controlling for whole-brain white matter with age, suggesting age-related trajectories unique to short range white matter connections. Furthermore, our results are in concert with those from a prior investigation of short range WM development that showed age-related increases in FA and decreases in MD and RD across the cerebrum in a healthy sample of children aged 10–18 years (Wu et al., 2014). Taken together, our findings suggest that short range WM continues to develop during childhood and adolescence, with the most robust differences occurring in the frontal, parietal, and temporal lobes.

During normal WM development, FA is shown to increase along with decreases in MD and RD as the brain matures from childhood to adulthood [Barnea-Goraly et al., 2005; Eluvathingal et al., 2007; Lebel and Beaulieu, 2011; Lebel et al., 2008; Mukherjee et al., 2001]. The converse is true in later life; decreases in FA along with increases in MD and RD are typically observed owing to normal declines in the microstructural constituency of WM [Westlye et al., 2009; Lebel et al., 2012; Phillips et al., 2013]. Though the biological determinants of diffusion parameters are not fully understood, increases in FA along with decreases in MD have been associated with greater maturation of long-range white matter connections in healthy children and adolescents [Barnea-Goraly et al., 2005; Eluvathingal et al., 2007; Lebel and Beaulieu, 2011; Lebel et al., 2008] while decreases in RD have been related to improved myelination and axonal packing of these tracts [Beaulieu et al., 2002; Song et al., 2005]. In line with

**TABLE III. Age-related changes in (a) whole-lobe and (b) hemispheric DTI measures across the brain for participants in the primarily longitudinal cohort**

a								
DTI measure	Intercept	Slope	SE	$R^2$	$P$	$q$		
FA								
Frontal	0.324	0.0031	0.0009	0.25	0.002	<b>0.034</b>		
Parietal	0.356	0.0031	0.0013	0.15	0.027	0.110		
Temporal	0.282	0.0034	0.0014	0.21	0.017	0.110		
Occipital	0.235	0.0034	0.0015	0.17	0.024	0.110		
MD	mm <sup>2</sup> /s	mm <sup>2</sup> /s/year						
Frontal	0.0008	$-6.06 \times 10^{-6}$	$2.27 \times 10^{-6}$	0.23	0.087	0.200		
Parietal	0.0007	$-4.17 \times 10^{-6}$	$2.59 \times 10^{-6}$	0.11	0.224	0.282		
temporal	0.0008	$-5.35 \times 10^{-6}$	$2.38 \times 10^{-6}$	0.18	0.122	0.243		
Occipital	0.0008	$-4.01 \times 10^{-6}$	$2.33 \times 10^{-6}$	0.13	0.208	0.282		
AD	mm <sup>2</sup> /s	mm <sup>2</sup> /s/year						
Frontal	0.0010	$-4.60 \times 10^{-6}$	$3.05 \times 10^{-6}$	0.14	0.229	0.282		
Parietal	0.0011	$-3.62 \times 10^{-6}$	$2.95 \times 10^{-6}$	0.13	0.308	0.352		
Temporal	0.0011	$-3.15 \times 10^{-6}$	$3.39 \times 10^{-6}$	0.04	0.414	0.442		
Occipital	0.0010	$-1.99 \times 10^{-6}$	$2.98 \times 10^{-6}$	0.08	0.553	0.553		
RD	mm <sup>2</sup> /s	mm <sup>2</sup> /s/year						
Frontal	0.0006	$-6.44 \times 10^{-6}$	$2.04 \times 10^{-6}$	0.22	0.065	0.200		
Parietal	0.0006	$-4.57 \times 10^{-6}$	$2.61 \times 10^{-6}$	0.11	0.201	0.282		
Temporal	0.0007	$-6.21 \times 10^{-6}$	$2.12 \times 10^{-6}$	0.19	0.088	0.200		
Occipital	0.0007	$-4.38 \times 10^{-6}$	$2.27 \times 10^{-6}$	0.09	0.186	0.282		
b								
DTI measure	<i>Left hemisphere</i>				<i>Right hemisphere</i>			
	Intercept	Slope	$R^2$	$q$	Intercept	Slope	$R^2$	$q$
FA								
Frontal	0.331	0.0035	0.27	<b>0.03</b>	0.320	0.0027	0.18	0.13
Parietal	0.347	0.0046	0.25	<b>0.03</b>	0.364	0.0017	0.05	0.71
Temporal	0.281	0.0048	0.28	<b>0.03</b>	0.278	0.0023	0.14	0.26
Occipital	0.281	0.003	0.10	0.24	0.178	0.0038	0.27	0.21
MD	mm <sup>2</sup> /s	mm <sup>2</sup> /s/yr ( $\times 10^{-6}$ )			mm <sup>2</sup> /s	mm <sup>2</sup> /s/yr ( $\times 10^{-6}$ )		
Frontal	0.00073	-6.53	0.27	0.25	0.0008	-5.57	0.19	0.25
Parietal	0.00074	-5.44	0.14	0.26	0.00076	-3.09	0.08	0.42
Temporal	0.00084	-5.37	0.16	0.25	0.00084	-5.29	0.20	0.25
Occipital	0.00075	-5.53	0.14	0.25	0.00087	-1.74	0.05	0.60
AD	mm <sup>2</sup> /s	mm <sup>2</sup> /s/yr ( $\times 10^{-6}$ )			mm <sup>2</sup> /s	mm <sup>2</sup> /s/yr ( $\times 10^{-6}$ )		
Frontal	0.001	-4.96	0.18	0.31	0.001	-4.20	0.10	0.39
Parietal	0.001	-3.43	0.10	0.42	0.001	-3.81	0.16	0.39
Temporal	0.001	-1.90	0.02	0.65	0.001	-4.32	0.06	0.39
Occipital	0.00095	-4.98	0.14	0.30	0.00097	0.92	0.06	0.79
RD	mm <sup>2</sup> /s	mm <sup>2</sup> /s/yr ( $\times 10^{-6}$ )			mm <sup>2</sup> /s	mm <sup>2</sup> /s/yr ( $\times 10^{-6}$ )		
Frontal	0.00058	-7.04	0.27	0.24	0.00067	-6.02	0.19	0.24
Parietal	0.00059	-6.55	0.19	0.25	0.00060	-2.84	0.06	0.45
Temporal	0.00071	-7.03	0.21	0.24	0.00071	-5.07	0.15	0.26
Occipital	0.00062	-5.44	0.13	0.25	0.00079	-2.16	0.13	0.55

SE—Standard error of slope.

$q$ —FDR-adjusted  $p$ -values. Values that survived FDR correction are bolded.

previous studies examining white matter growth, results from this study showed greater maturation of short range white matter in frontal, parietal, and temporal areas as evidenced by larger FA and smaller MD values with age. Smaller RD values with age in these areas suggest that

greater short range white matter maturation may be driven by increased myelination and axonal packing. Furthermore, we validated these maturational changes in a primarily longitudinal sample where we found age-related increases in FA in the frontal, parietal, and temporal lobes

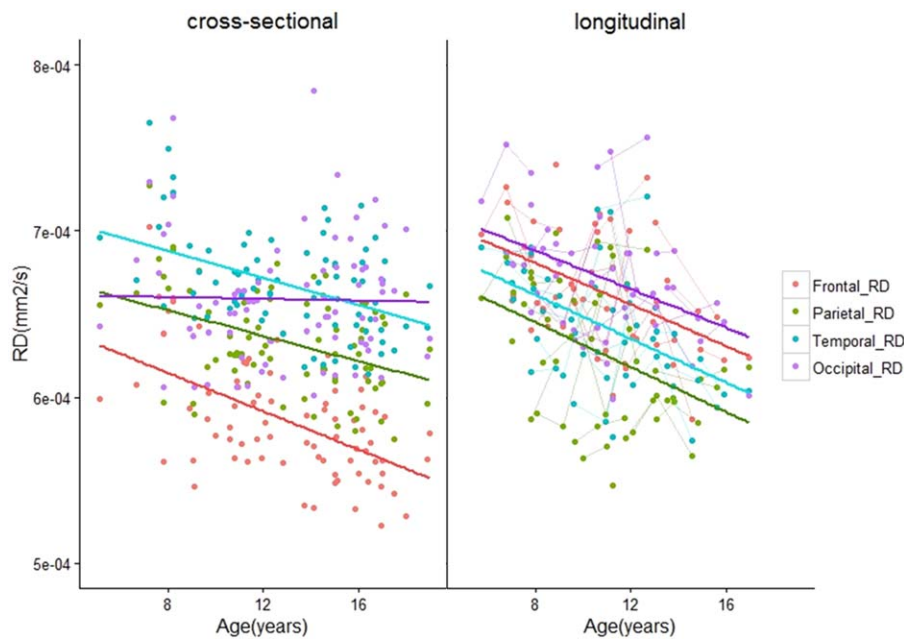


**Figure 7.**

Age-related changes in RD of short range WM across the brain. As with FA and MD, there were no age-related changes in RD in the occipital lobes of participants in the cross-sectional cohort. [Color figure can be viewed at [wileyonlinelibrary.com](http://wileyonlinelibrary.com)]

of the left hemisphere. By controlling for the effects of overall brain white matter with age we were able to delineate developmental trajectories unique to short-range white matter connections. Though participants in the cross-sectional cohort were older than those in the primarily longitudinal cohort, which may have led to higher DTI parameter values for participants in the cross-sectional cohort, it is notable that significant age-related maturation was observed in the frontal, parietal, and temporal lobes of both cohorts.

It is not surprising that age-related changes in short-range WM fibers in children and adolescents were best described by linear trajectories. Developmental increases in FA and decreases in MD and RD of long-range and regional white matter show nonlinear developmental trajectories characterized by initial linear increases in FA (or decreases in MD and RD) followed by a plateau in mid-adulthood, and decreases in FA (or increases in MD and RD) during normal aging [Lebel et al., 2008; Lebel and Beaulieu, 2011; Phillips et al., 2013; Westlye et al., 2009]. Similarly, we observed strong age-related linear increases in FA and decreases in MD and RD in our sample of children and adolescents. While these changes may mirror the initial linear trajectories associated with long-range fibers, future work looking at the maturation of short-range WM in a longitudinal sample of younger and older adults is required to ascertain whether short-range WM follows similar life-long trajectories as those of long-range WM fibers.

Qualitatively we observed that short range WM in frontal and temporal areas showed the greatest age-related differences in terms of slope while parietal areas showed less robust age-related maturation. As well, we did not observe any significant age-related changes in short-range WM within the occipital lobes. These observations are consistent with prior reports suggesting that brain development proceeds in a posterior-to-anterior sequence where posterior areas devoted to more basic functions develop early on while anterior areas associated with more complex functions mature later [Gogtay et al., 2004; Shaw et al., 2008]. Indeed, this pattern of development suggests that more anterior areas of the brain show greater change, especially during critical periods such as childhood and adolescence, where complex behavioral, cognitive, and emotional functions are being refined [Passler et al., 1985; Romine and Reynolds, 2005]. Complex behavioral processes are a product of interactive communication between local and distributed brain systems connected by processing networks comprised of short distance WM tracts [Mesulam, 1990]. These networks integrate incoming multimodal information and promote feedback processing of outgoing information [Mesulam, 1990]. Greater myelination and organization of short range WM in more anterior brain areas may support the integration of incoming information by enabling faster and more efficient transfer of information as children gain more experience and training during development. Moreover, myelination is promoted

by electrical impulses across axons [Demerens et al., 1996; Ishibashi et al., 2006], suggesting that increased activity in frontal and temporal areas during childhood/adolescence may also contribute to the maturational increases captured in diffusion parameter estimates.

Conversely, the relative absence of age-related maturation in the occipital lobes suggests that short range WM in these areas may mature early—perhaps related to the rapid maturation of visual areas in the first few years of life [Nomura et al., 1994]. In particular, the greatest maturation of short range WM in the occipital lobes may have occurred prior to the age of the youngest participant studied here (5.15 years). Our qualitative comparisons suggest that longitudinal designs may be most sensitive to any subtle age-related changes in occipital short range WM in older children and adolescents.

Findings of larger differences in FA in the frontal, parietal, and temporal lobes were lateralized to the left hemisphere. There is some evidence supporting left > right structural asymmetry in white matter of healthy individuals [Eluvathingal et al., 2007; Good et al., 2001; Phillips et al., 2013], with these differences more pronounced in males than females [Good et al., 2001]. The prominent leftward asymmetry in our results may reflect the greater number of MR measurements from males in both cohorts, although it is important to stress that we did not find any significant effects of sex on DTI measures.

Increased microstructural complexity of short-range WM with age in the left hemisphere may also reflect hemispheric differences in the organization of structural brain networks as children develop into young adults. As the human brain adapts to increasingly complex environmental demands, brain organization is shaped by the competing demands of cost-effective local communication driven by short-range connections within modules, and expensive inter-regional network communication driven by long-range connections [Bullmore and Sporns, 2012]. The development of structural brain organization from infancy to adolescence shows a marked decrease in the number of modules present in the brain with age, along with a simultaneous increase in global network communication [Dennis et al., 2013; Fan et al., 2011; Huang et al., 2013; Khundrakpam et al., 2012]. This suggests that as children get older the brain may prioritize effective inter-regional communication over less-expensive local communication subserved by short-range connections. Moreover, reductions in the number of modules have also been associated with an increase in the efficiency of intra-regional network communication, suggesting that short-range connections may become more fine-tuned with age [Hagmann et al., 2010; Huang et al., 2013]. Therefore, larger age-related changes in FA in the left hemisphere may reflect a more pronounced re-organization of structural brain modules in these areas during childhood and adolescence, though further neuroimaging studies are required to adequately characterize the nature of these changes within specific structural brain modules during development.

We consider our findings in the context of the following limitations. Although linear age effects on short range WM may reflect maturation in our sample of participants, a larger number of repeated within-subject scans may show nonlinear development trajectories, particularly for anterior brain areas. Indeed, prior developmental studies have highlighted the importance of longitudinal cohorts in the assessment of WM development in children and adolescents. It will be important for future studies to incorporate larger numbers of within-subject scans in order to fully characterize the developmental trajectories of short range WM. In terms of our MR acquisition approach, imaging data for both cohorts were acquired using scanners at different field strengths. Some studies have shown that FA values are statistically higher in 3 Tesla compared to 1.5 Tesla datasets [Huisman et al., 2006]. However, the majority of the WM development studies discussed here have utilized data acquired with 1.5 Tesla scanners. It is therefore notable that despite acquiring our data on both 3 and 1.5 Tesla scanners, we observed similar age-related changes in WM across field strengths. In terms of our imaging approach, the sequential elimination of probabilistic streamlines may not completely prevent signal contamination from the terminal ends of long range WM fibers. Future studies that use more sophisticated imaging techniques such as diffusion kurtosis imaging [Jensen et al., 2005] could resolve areas of crossing or overlapping fibers between short and long-range fibers and better delineate short-range white matter anatomy.

We have demonstrated the maturation of short range WM with age in frontal, temporal, and parietal areas in a healthy sample of children and adolescents. Age-related changes in the frontal, parietal, and temporal lobes were validated in a separate primarily longitudinal cohort of participants. These changes were lateralized to the left hemisphere, which may reflect the development of lateralized functions that is characteristic of this period of development. Our results are consistent with prior investigations of long range WM and extend currently limited work on the maturational trajectory of short range WM in the developing brain. Establishing a developmental model of age-related change in short range WM maturation is of benefit to researchers interested in the connectivity of large-scale neural networks, as well as clinicians interested in the contributions of these networks to neuropsychiatric diseases.

## ACKNOWLEDGMENTS

The authors thank Jovanka Skocic for technical assistance with image processing.

## CONFLICTS OF INTEREST

All authors on this manuscript have no conflicts of interests to disclose.

REFERENCES

- Assaf Y, Pasternak O (2008): Diffusion tensor imaging (DTI)-based white matter mapping in brain research: A review. *J Mol Neurosci* 34:51–61.
- Barnea-Goraly N, Menon V, Eckert M, Tamm L, Bammer R, Karchemskiy A, Dant CC, Reiss AL (2005): White matter development during childhood and adolescence: A cross-sectional diffusion tensor imaging study. *Cerebral Cortex* 15:1848–1854.
- Barr DJ, Levy R, Scheepers C, Tily HJ (2013): Random effects structure for confirmatory hypothesis testing: Keep it maximal. *J Mem Lang* 68:255–278.
- Basser PJ (1995): Inferring microstructural features and the physiological state of tissues from diffusion-weighted images. *NMR Biomed* 8:333–344.
- Basser PJ, Pajevic S, Pierpaoli C, Duda J, Aldroubi A (2000): In vivo fiber tractography using DT-MRI data. *Magn Reson Med* 44:625–632.
- Bates D, Mächler M, Bolker B, Walker S (2015): Fitting linear mixed-effects models using lme4. arXiv preprint arXiv:1406.5823.
- Beaulieu C (2002): The basis of anisotropic water diffusion in the nervous system—a technical review. *NMR in Biomedicine* 15: 435–455.
- Behrens T, Berg HJ, Jbabdi S, Rushworth M, Woolrich M (2007): Probabilistic diffusion tractography with multiple fibre orientations: What can we gain? *Neuroimage* 34:144–155.
- Behrens TE, Woolrich MW, Jenkinson M, Johansen-Berg H, Nunes RG, Clare S, Matthews PM, Brady JM, Smith SM (2003): Characterization and propagation of uncertainty in diffusion-weighted MR imaging. *Magn Reson Med* 50:1077–1088.
- Benjamini Y, Hochberg Y (1995): Controlling the false discovery rate: A practical and powerful approach to multiple testing. *J R Stat Soc Ser B (Methodological)* 289–300.
- Bolker BM, Brooks ME, Clark CJ, Geange SW, Poulsen JR, Stevens MHH, White JS (2009): Generalized linear mixed models: A practical guide for ecology and evolution. *Trends Ecol Evol* 24:127–135.
- Bullmore E, Sporns O. (2012): The economy of brain network organization. *Nat Rev Neurosci* 13:336.
- Catani M, Dell’Acqua F, Vergani F, Malik F, Hodge H, Roy P, Valabregue R, de Schotten MT (2012): Short frontal lobe connections of the human brain. *Cortex* 48:273–291.
- Demerens C, Stankoff B, Logak M, Anglade P, Allinquant B, Couraud F, Zalc B, Lubetzki C (1996): Induction of myelination in the central nervous system by electrical activity. *Proc Natl Acad Sci* 93:9887–9892.
- Dennis EL, Jahanshad N, McMahon KL, de Zubicaray GI, Martin NG, Hickie IB, Toga AW, Wright MJ, Thompson PM (2013): Development of brain structural connectivity between ages 12 and 30: A 4-Tesla diffusion imaging study in 439 adolescents and adults. *Neuroimage* 64:671–684.
- Eluvathingal TJ, Hasan KM, Kramer L, Fletcher JM, Ewing-Cobbs L (2007): Quantitative diffusion tensor tractography of association and projection fibers in normally developing children and adolescents. *Cerebr Cortex (New York, N.Y.)* 17:2760–2768.
- Fan Y, Shi F, Smith JK, Lin W, Gilmore JH, Shen D (2011): Brain anatomical networks in early human brain development. *Neuroimage* 54:1862–1871.
- Gogtay N, Giedd JN, Lusk L, Hayashi KM, Greenstein D, Vaituzis AC, Nugent TF 3rd, Herman DH, Clasen LS, Toga AW, Rapoport JL, Thompson PM (2004): Dynamic mapping of human cortical development during childhood through early adulthood. *Proc Natl Acad Sci U S A* 101:8174–8179.
- Good CD, Johnsrude I, Ashburner J, Henson RN, Friston KJ, Frackowiak RS (2001): Cerebral asymmetry and the effects of sex and handedness on brain structure: A voxel-based morphometric analysis of 465 normal adult human brains. *Neuroimage* 14:685–700.
- Hagmann P, Sporns O, Madan N, Cammoun L, Pienaar R, Wedeen VJ, Meuli R, Thiranb J-P, Grant PE (2010): White matter maturation reshapes structural connectivity in the late developing human brain. *Proc Natl Acad Sci* 107:19067–19072.
- Huang H, Shu N, Mishra V, Jeon T, Chalak L, Wang ZJ, Rollins N, Gong G, Cheng H, Peng Y, Dong Q, He Y (2013): Development of human brain structural networks through infancy and childhood. *Cerebr Cortex* 25:1389–1404.
- Huisman TA, Loenneker T, Barta G, Bellemann ME, Hennig J, Fischer JE, Il’yasov KA (2006): Quantitative diffusion tensor MR imaging of the brain: Field strength related variance of apparent diffusion coefficient (ADC) and fractional anisotropy (FA) scalars. *Eur Radiol* 16:1651.
- Ishibashi T, Dakin KA, Stevens B, Lee PR, Kozlov SV, Stewart CL, Fields RD (2006): Astrocytes promote myelination in response to electrical impulses. *Neuron* 49:823–832.
- Jenkinson M, Beckmann CF, Behrens TE, Woolrich MW, Smith SM (2012): Fsl. *Neuroimage* 62:782–790.
- Jensen JH, Helpert JA, Ramani A, Lu H, Kaczynski K (2005): Diffusional kurtosis imaging: The quantification of non-gaussian water diffusion by means of magnetic resonance imaging. *Magn Reson Med* 53:1432–1440.
- Khundrakpam BS, Reid A, Brauer J, Carbonell F, Lewis J, Ameis S, Karama S, Lee J, Chen Z, Das S, Evans AC (2012): Developmental changes in organization of structural brain networks. *Cerebr Cortex* 23:2072–2085.
- Le Bihan D, Mangin J, Poupon C, Clark CA, Pappata S, Molko N, Chabriat H (2001): Diffusion tensor imaging: Concepts and applications. *J Magn Reson Imaging* 13:534–546.
- Lebel C, Beaulieu C (2011): Longitudinal development of human brain wiring continues from childhood into adulthood. *J Neurosci* 31:10937–10947.
- Lebel C, Gee M, Camicioli R, Wieler M, Martin W, Beaulieu C (2012): Diffusion tensor imaging of white matter tract evolution over the lifespan. *Neuroimage* 60:340–352.
- Lebel C, Walker L, Leemans A, Phillips L, Beaulieu C (2008): Microstructural maturation of the human brain from childhood to adulthood. *Neuroimage* 40:1044–1055.
- Mabbott DJ, Rovet J, Noseworthy MD, Smith ML, Rockel C (2009): The relations between white matter and declarative memory in older children and adolescents. *Brain Res* 1294:80–90.
- Mazziotta J, Toga A, Evans A, Fox P, Lancaster J, Zilles K, Woods R, Paus T, Simpson G, Pike B, Holmes C, Collins L, Thompson P, MacDonald D, Iacoboni M, Schormann T, Amunts K, Palomero-Gallagher N, Geyer S, Parsons L, Narr K, Kabani N, Le Goualher G, Boomsma D, Cannon T, Kawashima R, Mazoyer B (2001): A probabilistic atlas and reference system for the human brain: International consortium for brain mapping (ICBM). *Philos Trans R Soc Lond B Biol Sci* 356:1293–1322.
- Mesulam M (1990): Large-scale neurocognitive networks and distributed processing for attention, language, and memory. *Ann Neurol* 28:597–613.
- Meynert T (1885): *Psychiatry—Clinical Treatise on Diseases of the Fore-Brain Based Upon a Study of its Structure, Functions, and Nutrition* (B. sachs, trans.). New York: Putnam,
- Mukherjee P, Miller JH, Shimony JS, Conturo TE, Lee BC, Almlil CR, McKinstry RC (2001): Normal brain maturation during

- childhood: Developmental trends characterized with diffusion-tensor MR imaging 1. *Radiology* 221:349–358.
- Nagy Z, Westerberg H, Klingberg T (2004): Maturation of white matter is associated with the development of cognitive functions during childhood. *J Cogn Neurosci* 16:1227–1233.
- Nazeri A, Chakravarty MM, Rajji TK, Felsky D, Rotenberg DJ, Mason M, Xu LN, Lobaugh NJ, Mulsant BH, Voineskos AN (2015): Superficial white matter as a novel substrate of age-related cognitive decline. *Neurobiol Aging* 36:2094–2106.
- Nomura Y, Sakuma H, Takeda K, Tagami T, Okuda Y, Nakagawa T (1994): Diffusional anisotropy of the human brain assessed with diffusion-weighted MR: Relation with normal brain development and aging. *Am J Neuroradiol* 15:231–238.
- Passler MA, Isaac W, Hynd GW (1985): Neuropsychological development of behavior attributed to frontal lobe functioning in children. *Dev Neuropsychol* 1:349–370.
- Phillips OR, Clark KA, Luders E, Azhir R, Joshi SH, Woods RP, Mazziotta JC, Toga AW, Narr KL (2013): Superficial white matter: Effects of age, sex, and hemisphere. *Brain Connectivity* 3:146–159.
- Romine CB, Reynolds CR (2005): A model of the development of frontal lobe functioning: Findings from a meta-analysis. *Appl Neuropsychol* 12:190–201.
- Shaw P, Kabani NJ, Lerch JP, Eckstrand K, Lenroot R, Gogtay N, Greenstein D, Clasen L, Evans A, Rapoport JL, Giedd JN, Wise SP (2008): Neurodevelopmental trajectories of the human cerebral cortex. *J Neurosci* 28:3586–3594.
- Smith SM, Jenkinson M, Woolrich MW, Beckmann CF, Behrens TE, Johansen-Berg H, Bannister PR, De Luca M, Drobnjak I, Flitney DE, Niazy RK, Saunders J, Vickers J, Zhang Y, De Stefano N, Brady JM, Matthews PM (2004): Advances in functional and structural MR image analysis and implementation as FSL. *Neuroimage* 23:S208–S219.
- Song S, Sun S, Ju W, Lin S, Cross AH, Neufeld AH (2003): Diffusion tensor imaging detects and differentiates axon and myelin degeneration in mouse optic nerve after retinal ischemia. *Neuroimage* 20:1714–1722.
- Song S, Sun S, Ramsbottom MJ, Chang C, Russell J, Cross AH (2002): Demyelination revealed through MRI as increased radial (but unchanged axial) diffusion of water. *Neuroimage* 17:1429–1436.
- Song S, Yoshino J, Le TQ, Lin SJ, Sun SW, Cross AH, Armstrong RC (2005): Demyelination increases radial diffusivity in corpus callosum of mouse brain. *Neuroimage* 26:132–140.
- Sowell ER, Thompson PM, Holmes CJ, Jernigan TL, Toga AW (1999): In vivo evidence for post-adolescent brain maturation in frontal and striatal regions. *Nat Neurosci* 2:859–861.
- Sporns O (2013). The human connectome: origins and challenges. *Neuroimage* 80:53–61.
- Thompson PM, Giedd JN, Woods RP, MacDonald D, Evans AC, Toga AW (2000): Growth patterns in the developing brain detected by using continuum mechanical tensor maps. *Nature* 404:190–193.
- Westlye LT, Walhovd KB, Dale AM, Bjørnerud A, Due-Tønnessen P, Engvig A, Grydeland H, Tamnes CK, Ostby Y, Fjell AM (2009): Life-span changes of the human brain white matter: Diffusion tensor imaging (DTI) and volumetry. *Cereb Cortex* 20:2055–2068.
- Woods RP, Grafton ST, Holmes CJ, Cherry SR, Mazziotta JC (1998): Automated image registration: I. general methods and intrasubject, intramodality validation. *J Comput Assist Tomogr* 22:139–152.
- Woolrich MW, Jbabdi S, Patenaude B, Chappell M, Makni S, Behrens T, Beckmann C, Jenkinson M, Smith SM (2009): Bayesian analysis of neuroimaging data in FSL. *Neuroimage* 45:S173–S186.
- Wu M, Lu LH, Lowes A, Yang S, Passarotti AM, Zhou XJ, Pavuluri MN (2014): Development of superficial white matter and its structural interplay with cortical gray matter in children and adolescents. *Hum Brain Mapp* 35:2806–2816.
- Yeterian EH, Pandya DN, Tomaiuolo F, Petrides M (2012): The cortical connectivity of the prefrontal cortex in the monkey brain. *Cortex* 48:58–81.
- Yekutieli D, Benjamini Y (1999): Resampling-based false discovery rate controlling multiple test procedures for correlated test statistics. *J Stat Plan Inference* 82:171–196.
- Zhang Y, Brady M, Smith S (2001): Segmentation of brain MR images through a hidden markov random field model and the expectation-maximization algorithm. *IEEE Trans Med Imaging* 20:45–57.